Published in final edited form as:

Pain. 2019 November ; 160(11): 2473–2486. doi:10.1097/j.pain.0000000000001648.

Assessment of nociception and related quality of life measures in a porcine model of Neurofibromatosis type 1

Rajesh Khanna[1,*], **Aubin Moutal**[1,a], **Katherine A. White**[2,a], **Aude Chefdeville**[1], **Pedro Negrao de Assis**[2], **Song Cai**[1], **Vicki J. Swier**[2], **Shreya S. Bellampalli**[1], **Marissa D. Giunta**[1], **Benjamin W. Darbro**[3,4], **Dawn E. Quelle**[4,5,6,7], **Jessica C. Sieren**[8,9], **Margaret R. Wallace**[10,11], **Christopher S. Rogers**[12], **David K. Meyerholz**[6], **Jill M. Weimer**[2,13]

[1]Department of Pharmacology, College of Medicine, University of Arizona, Tucson, Arizona 85724, USA;

[2]Pediatrics and Rare Diseases Group, Sanford Research, Sioux Falls, SD USA;

[3]Department of Pediatrics, University of Iowa Carver College of Medicine, Iowa City, IA, USA;

[4]Holden Comprehensive Cancer Center, University of Iowa, Iowa City, IA, USA;

[5]Molecular Medicine Program, University of Iowa Carver College of Medicine, Iowa City, IA, USA;

[6]Department of Pathology, University of Iowa Carver College of Medicine, Iowa City, IA, USA,

[7]Department of Pharmacology, University of Iowa Carver College of Medicine, Iowa City, IA, USA;

[8]Department of Radiology, University of Iowa Carver College of Medicine, Iowa City, IA, USA;

[9]Department of Biomedical Engineering at the University of Iowa, Iowa City, IA, USA;

[10]Dept. of Molecular Genetics and Microbiology, Univ. of Florida, Gainesville FL, USA;

[11]University of Florida Health Cancer Center, and UF Center for Neurogenetics, Univ. of Florida, Gainesville FL, USA;

[12]Exemplar Genetics, Coralville, IA, USA;

[13]Department of Pediatrics, Sanford School of Medicine, University of South Dakota, Sioux Falls SD USA

Keywords

Porcine; *NF1*$^{+/ex42del}$; Neurofibromatosis type 1; NF1; CRMP2 modifications; Cyclin-dependent kinase 5 phosphorylation; pain; sleep quality

[*]To whom correspondence should be addressed: Dr. Rajesh Khanna, Department of Pharmacology, College of Medicine, University of Arizona, 1501 North Campbell Drive, P.O. Box 245050, Tucson, AZ 85724, USA Office phone: (520) 626-4281; Fax: (520) 626-2204; rkhanna@email.arizona.edu.
[a]Equal contribution

Conflict of interest –
Dr. Chris Rogers is an employee of Exemplar Genetics. There is no conflict of interest for any of the other authors.

1. Introduction

Neurofibromatosis type 1 (NF1) is a human autosomal dominant genetic disorder resulting from germline mutations in the *NF1* gene [13; 30; 69; 70]. The *NF1* gene on chromosome 17q11.2 encodes the 320kDa cytoplasmic protein Neurofibromin. Neurofibromin is ubiquitously expressed, including during development [19], with highest expression in nervous system tissues [20]. Neurofibromin acts as a negative regulator of the protooncogene Ras activity through its RAS-GTPase activating domain [4; 78]. Therefore, impaired neurofibromin function increases Ras activation and stimulates downstream RAF/MEK and AKT/mTOR signaling pathways [18]. Neurofibromin also acts as an adenyl cyclase activity regulator [67], and may have other functions not yet characterized.

People with NF1 can experience a variety of symptoms, including pigmentary abnormalities (café-au-lait macules, axillary/inguinal freckling) [33], skeletal deformities, cardiovascular abnormalities, and cognitive deficits (attention and learning impairments) [34]. Individuals with NF1 are prone to develop benign, and occasionally malignant, tumors of the central and peripheral nervous system. About 15% of children with NF1 develop a glioma of the optic pathway [45] and adults bear a 50–100-fold increased risk of developing a malignant glioma compared to the general population [31]. NF1 patients are also at high risk for the development of malignant peripheral nerve sheath tumors (MPNSTs), which are the leading cause of death in this patient population [24; 61]. Finally, patients with this disease report experiencing abnormal levels of pain [5; 40]: ~68% of adults with NF1 experience pain regularly, ~48% reported chronic pain lasting for more than 3 months, ~58% suffered from high frequency pain [40]. The most commonly prescribed medication to manage NF1 pain is gabapentin [40], which targets and inhibits the α2-δ subunit of the voltage gated calcium channel CaV2.2 [25].

In the 1990s, mouse strains harboring mutations in *Nf1* were created to model NF1, as there are no naturally-occurring animal models of NF1. Heterozygous $Nf1^{+/-}$ mice generated by multiple groups either presented with no obvious abnormalities [7], moderate learning and memory impairments [63], and predisposition to spontaneous tumors, such as myeloid leukemia [37; 77]. None of these mice developed neurofibromas, the hallmark tumor of the disease. Later work showed that targeted inactivation of *Nf1* in desert hedgehog-expressing cells during development led to formation of dermal and plexiform neurofibromas [74]. CNS tumors were also observed following co-inactivation of *Nf1* with other tumor suppressor genes, such as *p53* or Phosphatase and tensin homolog (*Pten*), in neuroglial precursors [42; 80].

In an attempt to generate a large animal model of NF1, miniswine harboring a disruptive *NF1* mutation on either exon 42 [74] or exon 41 [36] of the pig *NF1* gene were engineered. These miniswine spontaneously exhibited café-au-lait macules, learning impairment and neurofibromas, thus recapitulating classic features of NF1, many of which are not displayed in conventional heterozygotic rodent models [36; 74]. However, pain perception and signaling in NF1 have not been investigated in these models [5]. Here, we: *(i)* have developed novel tools to monitor behaviors related to pain in NF1-mutant miniswine and *(ii)* demonstrate the translational potential of two pharmacological approaches to reverse

calcium channel dysregulation in NF1. We suggest that pain modeling in large animals, such as pigs, offers considerable translational potential for driving therapeutic discoveries.

2. Methods

2.1. Culturing of miniswine DRG neurons.

DRG neurons were isolated from 7–9-month-old Yucatan miniswine at necropsy using bilateral laminectomy approach as described previously [50; 74]. Briefly, the skin and epaxial muscles overlying the distal thoracic to lumbar spine were excised. The spine was transected at approximately T12 to expose the spinal canal. Vertebral laminae were bilaterally sectioned to remove the dorsal covering of the lumbar spinal canal. Dorsal roots of the spinal nerves were sectioned at the level of the spinal cord and deep within the neuroforamina to excise intact DRGs. After dissection, DRGs were sent in DMEM media, by overnight shipping, on wet ice from Iowa to the university of Arizona. DRGs were digested in 3 ml neurobasal media (Cat# 21103049, ThermoFisher Scientific) containing collagenase Type II (Cat# LS004205, Thermofisher, 12 mg/ml) and dispase II (Cat# 17-105-041, Thermofisher, 20 mg/ml) and incubated for 45–75 minutes at 37°C under gentile agitation. Dissociated DRG neurons (~1.5×10^6) were then gently centrifuged to collect cells and washed with and grown in Neurobasal media containing 1% penicillin/streptomycin sulfate from 10,000 μg/ml stock, 30 $ng.ml^{-1}$ nerve growth factor (Thermofisher), 10% FBS (Hyclone) and 2% B-27 (Cat# 17-504-044, Thermofisher).

2.2. Calcium imaging in acutely dissociated miniswine DRG neurons.

Dorsal root ganglion neurons were loaded for 30 minutes at 37°C with 3 μM Fura-2AM (Cat# F1221, Thermo Fisher, stock solution prepared at 1mM in DMSO, 0.02% pluronic acid, Cat#P-3000MP, Life Technologies) to follow changes in intracellular calcium($[Ca^{2+}]_c$) in a standard bath solution containing 139 mM NaCl, 3 mM KCl, 0.8 mM $MgCl_2$, 1.8 mM $CaCl_2$, 10 mM Na HEPES, pH 7.4, 5 mM glucose exactly as previously described [8]. Fluorescence imaging was performed with an inverted microscope, NikonEclipseT*i*-U (Nikon Instruments Inc., Melville, NY), using objective Nikon Fluor 4X and a Photometrics cooled CCD camera Cool SNAP ES^2 (Roper Scientific, Tucson, AZ) controlled by Nis Elements software (version 4.20, Nikon Instruments). The excitation light was delivered by a Lambda-LS system (Sutter Instruments, Novato, CA). The excitation filters (340 ± 5 and 380 ± 7) were controlled by a Lambda 10 to 2 optical filter change (Sutter Instruments). Fluorescence was recorded through a 505-nm dichroic mirror at 535 ± 25 nm. To minimize photobleaching and phototoxicity, the images were taken every ~10 seconds during the time-course of the experiment using the minimal exposure time that provided acceptable image quality. The changes in $[Ca^{2+}]_c$ were monitored by following a ratio of F_{340}/F_{380}, calculated after subtracting the background from both channels.

2.3. Whole-cell patch recordings of Ca^{2+} currents in acutely dissociated miniswine DRG neurons.

Recordings were obtained from acutely dissociated small to medium diameter (ø<50–70μm; calculated from staining of the ganglia with β-III tubulin (data not shown) as well as inferred from a published study [50]) DRG neurons as described previously [35; 56]. To isolate

calcium currents, Na^+ and K^+ currents were blocked with 500 nM tetrodotoxin (TTX; Alomone Laboratories) and 30 mM tetraethylammonium chloride (TEA-Cl; Sigma). Extracellular recording solution (at ~310 mOsm) consisted of the following (in mM): 110 *N*-methyl-D-glucamine (NMDG), 10 $BaCl_2$, 30 TEA-Cl, 10 HEPES, 10 glucose, pH at 7.4, 0.001 TTX, 0.01 nifedipine. The intracellular recording solution (at ~310 mOsm) consisted of the following (in mM): 150 $CsCl_2$, 10 HEPES, 5 Mg-ATP, 5 BAPTA, pH at 7.4. Activation of I_{Ca} was measured by using a holding voltage of −90 mV with voltage steps 200 milliseconds in duration applied at 5-second intervals in + 10 mV increments from −70 to +60 mV. Current density was calculated as peak I_{Ca}/cell capacitance. Steady-state inactivation of I_{Ca} was determined by applying an 800-millisecond conditioning prepulse (−100 to −20mV in +10mV increments) after which the voltage was stepped to −20 mV for 200 milliseconds; a 15-second interval separated each acquisition. Whole-cell voltage clamp recordings were performed at room temperature using an EPC 10 Amplifier-HEKA as previously described [23]. The internal solution for voltage clamp sodium current recordings contained (in mM): 140 CsF, 1.1 CsEGTA, 10 NaCl, and 15 HEPES (pH 7.3, 290–310 mOsm/L) and external solution contained (in mM): 140 NaCl, 3 KCl, 30 tetraethylammonium chloride, 1 $CaCl_2$, 0.5 $CdCl_2$, 1 $MgCl_2$, 10 D-glucose, and 10 HEPES (pH 7.3, 310–315 mOsm/L).

Fire-polished recording pipettes, 2 to 5 MΩ resistance were used for all recordings. Whole-cell recordings were obtained with a HEKA EPC-10 USB (HEKA Instruments Inc., Bellmore, NY); data were acquired with a Patchmaster (HEKA) and analyzed with a Fitmaster (HEKA). Capacitive artifacts were fully compensated, and series resistance was compensated by ~70%. Recordings made from cells with greater than a 5mV shift in series resistance compensation error were excluded from analysis. All experiments were performed at room temperature (~23°C).

The Boltzmann relation was used to determine the voltage dependence for activation of I_{Ca} and wherein the conductance-voltage curve was fit by the equation $G/G_{max} = 1/ [1 + \exp (V_{0.5} - V_m)/k]$, where G is the conductance $G=I/(V_m-E_{Ca})$, G_{max} is the maximal conductance obtained from the Boltzmann fit under control conditions, $V_{0.5}$ is the voltage for half-maximal activation, V_m is the membrane potential, and k is a slope factor. E_{Ca} is the reversal potential for I_{Ca}; E_{Na} is the reversal potential for I_{Na} and was determined for each individual neuron. The values of I_{Ca} and around the reversal potential were fit with a linear regression line to establish the voltage at which the current was zero. The Boltzmann parameters were determined for each individual neuron and then used to calculate the mean ± S.E.M.

2.4. Sample preparation for mass spectrometry.

DRGs were dissected from either wildtype or *NF1*$^{+/ex42del}$ *pigs* and flash frozen in dry ice. Samples were sent overnight from Iowa to the University of Arizona on dry ice. Proteins were extracted in 20 mM Tris, 50 mM NaCl, 2 mM $MgCl_2$, 1% Tergitol, 0.5% Sodium Deoxycholate, 0.1 % Sodium dodecyl sulfate with Protease (Cat# B14002, Bimake), phosphatase (Cat# B15002, Bimake) inhibitor cocktails and 5U/ml of Universal nuclease (Cat# 88702, Thermofisher) added extemporaneously. Tissues were disrupted by sonication

and lysates were then cleared by centrifugation at 10000xg for 10 min at 4°C. The concentration of lysates was measured by BCA (Cat# 23227, Thermofisher) and 100 μg of total protein (heat denatured and reduced with 100 mM DTT) was loaded on a SDS-PAGE 4–20% gradient gel (Cat# XP04205BOX, Thermofisher). After running, SDS-PAGE was stained with Bio-Safe Coomassie G-250 Stain (Cat# 1610786, Biorad) according to manufacturer's instructions. Six samples were run per gel and all twelve samples were processed simultaneously to minimize experimental variation. Each lane of the SDS-PAGE gel was cut to isolate the 50 to 75 kDa (determined by comparison with PageRuler™ Plus Prestained Protein Ladder, 10 to 250 kDa, Cat# 26620, Thermofisher) area containing our protein of interest CRMP2. The slices was further sliced into ~1mm cubes and placed in a 0.6 ml LoBind polypropylene tube (Cat# 13-698-793, Fisher) containing LCMS-H_20 prior to a 30 min incubation step at 37°C under agitation. Coomassie staining was destained by two 30 min incubation steps with 375 μl of 50% acetonitrile (ACN) in 40 mM NH_4HCO_3 at 37°C under agitation. Gel slices were then dehydrated with 100% ACN for 15 min at RT. The ACN was removed and the gel slices dried in a vacuum centrifuge (62°C for 30 min). Trypsin (Cat# 90058, Thermofisher) was added to the dried gel slices at 0.01μg/μl in 100 mM NH_4HCO_3 for a total of 0.5μg of trypin per sample. Dried gel slices were allowed rehydrate for 15 min at 4°C and 100 mM NH_4HCO_3 was added to the gel pieces until fully flooded. The trypsin digestion was done overnight at 37°C under agitation. The reaction was terminated by addition of 5% formic acid (FA) and incubation at 37 °C for 30 min. Samples were centrifuged at 12000xg for 1min and the supernatant harvested into a clean LoBind polypropylene tube. A second extraction step was done on the gel slices using 0.5% FA to ensure the maximum recovery of the digested peptides. Both supernatants were combined and dried in a vacuum centrifuge (62°C) until ~5–10 μl were left. After addition of 10 μl 0.05% heptafluorobutyric acid (HBFA)/5% FA (v/v) and incubation at room temperature for 15 min, the samples containing the peptides were loaded on a solid phase C18 ZipTip (Cat# ZTC18S096, Millipore, Billerica, MA) after preparing the ZipTip with ACN and washing with 0.005% HFBA/5% FA (v/v). Peptide loaded ZipTips were washed with 0.005% HBFA/5% FA (v/v) followed by two elution steps first using 50% ACN/1% FA (v/v) and second with 80% ACN/1% FA (v/v). The eluates were combined and dried completely by vacuum centrifugation. Peptides were then ressuspended in 0.1% FA (v/v) and brief sonication. Samples were kept at −80°C until analysis.

2.4.1. Mass Spectrometry and Data Processing.—HPLC-ESI-MS/MS was performed in positive ion mode on a Thermo Scientific Orbitrap Elite Velos Pro hybrid mass spectrometer fitted with an EASY-Spray Source (Thermo Scientific, San Jose, CA). NanoLC was performed using a Thermo Scientific UltiMate 3000 RSLCnano System with an EASY Spray C18 LC column (Thermo Scientific, 50 cm × 75 μm inner diameter, packed with PepMap RSLC C18 material, 2 μm, Cat. # ES803); loading phase for 15 min; mobile phase, linear gradient of 1–47% ACN in 0.1% FA in 106 min, followed by a step to 95% ACN in 0.1% FA over 5 min, hold 10 min, and then a step to 1% ACN in 0.1% FA over 1 min and a final hold for 19 min (total run 156 min); Buffer A = 100% H_2O in 0.1% FA; Buffer B = 100% ACN in 0.1% FA; flow rate, 300 nl/min. All solvents were liquid chromatography mass spectrometry grade. Spectra were acquired using XCalibur, version 2.1.0 (Thermo Scientific). A "top 15" data-dependent MS/MS analysis was performed (acquisition of a full

scan spectrum followed by collision-induced dissociation mass spectra of the 15 most abundant ions in the survey scan). Dynamic exclusion was enabled with a repeat count of 1, a repeat duration of 30 s, an exclusion list size of 500, and an exclusion duration of 40 s. Tandem mass spectra were extracted from Xcalibur "RAW" files and charge states were assigned using the ProteoWizard 2.1.x msConvert script using the default parameters [14]. The fragment mass spectra were then searched against the sus scrofa proteome (UP000008227) using Mascot (Matrix Science, London, UK; version 2.5.0) using the default probability cut-off score. The search variables that were used were: 10 ppm mass tolerance for precursor ion masses and 0.5 Daltons for product ion masses; digestion with trypsin; a maximum of two missed tryptic cleavages; variable modifications of oxidation of methionine and phosphorylation of serine, threonine, and tyrosine. Cross-correlation of Mascot search results with X! Tandem was accomplished with Scaffold (version Scaffold_4.4.0; Proteome Software, Portland, OR). For CRMP2 (Uniprot ID: I3LJE2), we detected 45 unique peptides and 5 phosphorylated peptides (2 for pS647, 2 for pS627 and 1 for pS27 considering only +2 and +3 charge) with <95% confidence. Phosphorylated peptide abundance (area under the curve calculated in Progenesis) was normalized on the total abundance of CRMP2 in each sample. Levels of phosphorylated CRMP2 were averaged for each genotype and analyzed using the Mann-Whitney test.

2.5. Assessment of Spontaneous Pain Behavior Using a Composite Behavior Scale and Home Pen Monitoring.

All animals were housed at Exemplar Genetics under an approved IACUC protocol (MRP2016–009), and their use in behavioral testing is noted in Supplementary Table 1. Due to the nature of using large animal models, Ns and ages were limited. All animals were group housed similar to what has been reported in some studies (for example, see [11]) at the time of testing except for one animal, which is noted in Supplementary Table 1. All boars had intact testes for the duration of the study. The solitary performance and social behavior of each animal was scored during a 10-minute observation period by a trained, facility caretaker as described previously as a means of monitoring overt, obvious signs of pain or distress. (Supplementary Table 2) [12]. Score driving parameters related to observing the animals' standing posture, leg guarding, leg shaking, as well as their vocalization and social behavior (isolation and aggressiveness). Each parameter was graded from 0 to 2, depending on the observed behavior. A higher score indicates that the animal expressed more spontaneous pain behavior. The maximum possible score was 11 points. Spontaneous expression scores were observed monthly as permissible (Adapted from [12]). Additionally, animals were monitored bi-monthly for indicators of tumor growth, blindness, loss of vision, body weight, body condition, seizures, limb paralysis, lethargy, feeding behavior, ability to bear body weight, vocalization, restlessness, agitation, aggression, and isolation.

Each animal was tracked for 6 days using a FitBark2 (www.fitbark.com) device, attached to their neck using a common dog or calf collar at 10–12 months of age. FitBark monitors allow us to record animals' activities without the influence of human interaction and have been used in sheep [59]. Readouts included: sleep quality, time spent being active, playing, and resting, distance travelled, and weight. Sleep quality represent a percentage of the time where animal's sleep is not interrupted by movements during a period where the animal is

usually asleep and is therefore a measure of sleep fragmentation. This allowed us to monitor the animals' activities without the influence of human interaction. At this time point, female wildtype animals were not available for testing, resulting in female NF1 mutant animals being compared to male wildtype animals. We faced some hurdles with the FitBark devices, as some animals did not wish to comply with the testing.; these animals would remove their collars and destroy the device after a few hours of wear. Attempts to change the collar to a harness, or to connect it around the animal's chest rather than the neck were unsuccessful in reducing this. As such, while we obtained strong data at 10–12 months and 20–22 months of age.

2.6. Assessment of Tactile Allodynia

In order to gauge an animal's level of pain/sensitivity, we monitored the animal's response to von Frey sensory probes (Stoelting 58011; probe range 0.008–300 grams) when stimulated on the skin of the anthelix (a part of the visible ear; the pinna. The antihelix is a curved prominence of cartilage parallel with and in front of the helix on the pinna) just inside the ear. Our studies on ear pinna skin did not include regions with tumors or macules. Animals were monitored for response to sensory probes over five consecutive trials stating at 1 gram of target force, with a positive response deemed as the animal responding at least three out of five trials (ear flick, facial muscle twitch, or similar response). If the animal responded to the 1-gram target force, lower pressure probes were used to stimulate the anthelix of the ear at five trials each, until the lowest target force that garnished a response was determined. If the animal did not respond to the 1-gram target force, higher pressure probes were used to stimulate the anthelix of the ear until at five trials each, until the highest target force that garnished a response was determined. The lowest target force detected by each animal was converted on a log2 scale (as the target probes are non-linear and animals perceive stimuli on a logarithmic scale (Weber's Law)) [51].

2.7. Thermal Laser Stimulation

Withdrawal reflex via thermal laser stimulation was modified based on Herskin et al. [32]. Animals were secured in a sling and a 2W S3 Arctic laser (Wicked Laser; http://www.wickedlasers.com/arctic) was used to stimulate three distinct areas of the back of the outer ear for three, 20 second trials at a distance of 100cm. With each distinct area, the latency to respond to the laser stimulation was recorded with a maximum respond time of 20 seconds, and the latency to respond to each trial was averaged into one value per animal. The original Herskin et al publication [32] stimulated the shoulder and leg, though we found our animals would not consistently respond to stimulation in those areas (data not shown).

2.8. Additional pain assessment protocols

Bright light, pigeon feather, and air puff tests were employed in an attempt to measure stimuli response in swine subjects secured in a sling.

2.8.1. Bright Light Exposure—An LED headlamp was affixed to the experimenter's head (Amazon B00H26CGTI) in a dark room, and the animal was exposed to a bright, flashing strobe light for five 15 second trials [38]. Avoidance response to the light was recorded.

2.8.2. Pigeon Feather Stimulation—A single, natural, 6–8-inch-long pigeon feather (Amazon B071JF1JFC) was gently brushed across various areas of the animal's face, such as the snout and undereye area, where skin was anticipated to be thinnest [62]. The response out of five trials was recorded.

2.8.3. Air Puff Stimulation—A 10cc syringe was placed 8–10 cm from the side of the animal's eye and a puff of air was directed at the eyelids [41]. The response out of five trials was recorded.

2.9. Study approval

All animals were maintained at Exemplar Genetics under an approved IACUC protocol (protocol no. MRP2016–009). DRG samples were obtained from individuals targeted for necropsy and sample were shared with multiple other labs at the University of Iowa in accordance with the IACUC approved protocol (Office of Animal Resources, University of Iowa; protocol no. 7061269).

2.10. Experimental Design and Statistical Measurement

All animals were randomly assigned to distinct experimental groups by an off-site experimenter. All technicians performing the behavior experiments were blinded to genotype, with all data analyzed by a blinded, off-site experimenter. Statistical tests are noted in the figure legends and include an unpaired student's t-test (pooled sexes) and an ordinary two-way ANOVA with a Tukey post-hoc correction (split sexes). Graphs are represented as scatter plots with mean ± SEM.

3. Results

3.1. $NF1^{+/ex42del}$ pigs exhibit reflexive allodynia and hyperalgesia as well as spontaneous pain behaviors in a sex- and time-dependent manner

We recently reported the generation of *$NF1^{+/ex42del}$* Yucatan miniature swine via recombinant adeno-associated virus-mediated gene targeting and somatic cell nuclear transfer methods [74]. As in patients with NF1, all affected swine were heterozygous. *$NF1^{+/ex42del}$* animals presented with spontaneous café au lait macules and neurofibromas, two classic disease phenotypes that are absent in heterozygous *Nf1* rodent models [74]. The *$NF1^{+/ex42del}$* miniswine also presented with initial learning delay in the T-maze task, an initial hesitance to interact with a novel object, and overall observations of hyperactivity and anxiety [74]. People with NF1 report idiopathic pain [17; 40] and we found that *Nf1* gene editing could directly result in allodynia in rats [52; 57; 58]. We asked if this was also true in our *NF1* mutant miniswine model. Since pain behavior testing in pigs has not been extensively attempted or studied, we first tried to replicate some of the classical rodent testing approaches for pain in the pigs. To this end, we employed a variety of techniques, including assessment of migraine-like light-aversion from a bright, flashing light [38]; gentle, non-contact tactile assessment of aversion as a puff of air was directed at the eye [41]; gentle, contact tactile sensitivity assessment using a pigeon feather stimulus near the eye [12]; and reaction to von Frey filaments just inside the ear. The light-aversion, air puff, and pigeon feather experiments were unsuccessful, as all animals regardless of genotype

reacted extremely quickly and similarly to the light-aversion and air puff tests, and animals did not respond to the pigeon feather experiment, likely due to their thick skin (data not shown).

In contrast, we were able to successfully measure the reaction to the von Frey filaments. In male *NF1*$^{+/ex42del}$ pigs, which form tumors at an average of 10.5 months of age, we observed a decrease in withdrawal threshold to von Frey filaments in tumor-burdened *NF1*$^{+/ex42del}$ pigs (Figure 1A). This sensitization occurred at 9 months of age and did not present upon subsequent testing at 12, 15, and 18 months of age. Neurofibromas were only observed in males, predominantly on their upper body (Table 1) where the animals tended to ram into each other or rub aggressively against each other or their pens. Similarly, when comparing age and gender-matched female animals, where female *NF1*$^{+/ex42del}$ pigs do not show any tumor growth [74], we observed a decrease in von Frey withdrawal threshold in *NF1*$^{+/ex42del}$ pigs at 9 months of age, a response that also disappeared upon subsequent testing at 12, 15, 18, 21, and 24 months of age (Figure 1B). Looking at all pigs regardless of sex, the combined data shows that *NF1*$^{+/ex42del}$ pigs have significant allodynia at 9 months of age, with tumor-burdened males showing a significantly lower threshold response than both wildtype controls and *NF1*$^{+/ex42del}$ animals without tumors (Figure 1C, D).

We recognized that the initial sensitivity to von Frey stimuli may have been an anxious or hyperactivity response rather than allodynia. Therefore, we also assessed spontaneous pain behaviors using a composite behavior scale reported by Meilin and colleagues [12]. In general, the parameters relate to observing the animals' standing posture, leg guarding, leg shaking, as well as their vocalization and social behavior (isolation and aggressiveness) (Supplemental Table 2). In this manner, the solitary performance and social behavior of each animal were scored during a 10-minute observation period by a trained, facility caretaker. There were no differences between genotypes in weight bearing, appearance, vocalization, restlessness, aggression, and isolation scores, as all animals scored 0 in these parameters (data not shown). While animals did score on agitation, there were similarly no differences between genotypes at 9 months of age, when differences in von Frey sensitivity were detected (Figure 1E). Taken together, this dataset shows that *NF1*$^{+/ex42del}$ pigs have features of hypersensitivity to tactile stimuli, as has been reported by NF1 patients [68] and in rodent models of NF1 [75]. Importantly, allodynia in NF1 mutant pigs is sex and tumor burden dependent. While *NF1*$^{+/ex42del}$ allodynia response to the von Frey filaments appeared to diminish over time, we interpret this as the animals simply becoming used to the testing paradigm over multiple rounds of testing. Therefore, future von Frey experiments in this swine model are recommended to employ infrequent von Frey testing to avoid testing fatigue in the animals.

Next, we used a laser-based method to measure thermal nociception [32] in wildtype and *NF1*$^{+/ex42del}$ pigs. Withdrawal reflex of the hindlegs and shoulders was recorded in response to a thermal stimulation with a handheld laser with 1–2 watts power output. This response did not differ between the genotypes (data not shown). The nociceptive response of the pigs, assessed by examining their reactions to a laser beam applied to the outer part of the ear at a distance of 100cm (Figure 2A), resulted in reflexive behavioral responses in all animals tested. Male wildtype and *NF1*$^{+/ex42del}$ pigs (with and without neurofibromas) (Table 1) at

12–15 months of age did not show any differences in their latencies to respond to the laser shone on the ear (Figure 2B). In contrast, female *NF1*$^{+/ex42del}$ pigs had significantly faster response times to the laser compared to age-matched wildtype female pigs (Figure 2C), further supporting a sex-based origin in NF1 swine model pain perception. This sensitization was generally consistent over multiple testing periods, with wildtype females becoming more sensitized to the laser stimulus after multiple rounds of testing. To our knowledge, there are no differences in adipose or collagen between WT and NF1 pig skin. The only detectable difference reported in our original characterization of the pigs [74] is a slight expansion in the size of the neurovascular networks within the upper dermis; neurovascular networks are spaces/channels where vessels and nerves normally reside, and these are seen in the dermis of skin in most species. We suspect this is due to the wildtype pigs learning the settings of this assay or to the skin becoming more sensitive to the laser stimulus after prolonged exposure to the laser. As such, similar to the von Frey measurements, we suspect that careful, intermittent laser testing is key to consistent measurements of thermal sensitivity in these swine models.

3.2. NF1$^{+/ex42del}$ pigs are affected in health-related quality of life domains

It has been previously shown that pain is associated with various comorbidities in health-related quality of life domains in NF1 patients [26]. For this reason, we used a FitBark monitoring device to assess sleep quality and activity related measures, such as percent of day active, resting, playing and total distance traveled, by wildtype and *NF1*$^{+/ex42del}$ pigs. While no significant differences were found between wildtype and male *NF1*$^{+/ex42del}$ pigs in measures of percent of day active (Figure 3A), playing (Figure 3B) or total distance traveled (km) (Figure 3C), the percent of day resting (Figure 3D) and sleep quality (Figure 3E) were adversely affected in *NF1*$^{+/ex42del}$ pigs compared to their wildtype counterparts at 10 to 12 months of age. Specifically, male *NF1*$^{+/ex42del}$ pigs with tumors rested longer than male wildtype pigs (Figure 3D). In contrast, sleep quality was reduced in the same male *NF1*$^{+/ex42del}$ pigs with tumors compared to wildtype male pigs (Figure 3E), even though these animals were spending more of their time resting. An older cohort (20–22 months) [because additional WT females were not available at 10–12 months of age] of wildtype and *NF1*$^{+/ex42del}$ pigs were also monitored for their sleep quality and activity related measures (Figure 3E). We observed that the older cohort of female pigs did not differ in their activity, playtime, rest, and sleep quality between genotypes (Figure 3A–E). Importantly, the values obtained for the quality of life parameters of the older female cohort (either genotype) were not different from those of the younger female cohort, which allows us to now conclude that the reduction in the quality of life – % of day resting and sleep quality – is linked to tumor burden in males and is not manifest in females as well as a lack of age dependency of the quality of life indices. Since no female pigs in our cohort developed tumors, we cannot make any conclusions on this particular data.

To determine if these quality of life measurements corresponded with our other behavioral assays, we ran a correlation analysis between NF1 mutant animals that had matching von Frey and FitBark data. Excitingly, there were significant correlations between higher sensitivity to von Frey stimuli and FitBark quality of life measurements (lower sleep quality; more time spent resting) (Figure 3F). Animals that presented with tumors (open circles and

squares) clustered around data points with high von Frey scores, more time resting, and lower sleep quality. While it is difficult to determine a correlation between sensitivity and location/size of the tumor based on this small sample number, there was one animal that appeared to transition to tumor formation during this time period (arrows). This animal did not have a tumor during the von Frey assessment, but presented with a tumor on its side during the FitBark analysis. Interestingly, this 'transitioning' animal scored less severely than the two other tumor-burdened animals on all three assays, suggesting perhaps that allodynia is directly linked to specific tumor burden. As a comparison, in healthy dogs, approximately 15% of a given sleep period is interrupted by movements, thus giving an 85% sleep quality (FitBark data), close to what is observed in our wildtype pigs. Taken together, these data establish disturbances in health-related quality of life domains in *NF1*$^{+/ex42del}$ pigs, consistent with reports of patients with NF1 with mental health and sleep issues and an overall poorer life satisfaction index, and establish a connection between allodynia and quality of life measures [26].

3.3. Characterization of ion channel remodeling NF1 mutant miniswine

Since previous reports have demonstrated an increase in voltage gated N-type Ca^{2+} (CaV2.2) channel current densities in neurons from *Nf1*$^{+/-}$ mice, placing CaV2.2 as the major contributor to whole cell Ca^{2+} currents in NF1, with no significant differences in L-, P/Q-, T- and R-type currents [22], we used whole-cell voltage-clamp electrophysiology to assess the activity of these channels in DRGs from wildtype and *NF1*$^{+/ex42del}$ pigs. Representative recordings from a small diameter sensory neuron from wildtype and *NF1*$^{+/ex42del}$ pigs are illustrated in Figure 4A.

To account for the variations in cell size, the calcium currents obtained from 10 wildtype and 5 *NF1*$^{+/ex42del}$ sensory neurons were normalized to cell capacitance and shown as the current density-voltage relation, summarized in Figure 4B. The cell capacitance for the isolated neurons was not different between the two genotypes (data not shown). There was an ~2.3-fold significant increase in the average peak current densities between wildtype compared to *NF1*$^{+/ex42del}$ neurons (−40.6 ± 5.4 vs. −94.3 ± 4.5 pA/pF, respectively, for steps to +10 mV, $p<0.05$, t-test) (Figure 4B, C). When the current values were transformed to conductance (G), the conductance-voltage relation was fit with the Boltzmann relation, and the conductance for each neuron was then normalized to the maximal value of G (Gmax) obtained from the fit. The G/Gmax-voltage relation is summarized in Figure 4D and indicates that the voltage-dependence for activation of Gmax was nearly identical between the two genotypes: the Boltzmann fitting parameters, voltage for half-maximal activation ($V_{0.5}$) and slope (k) were −26.3 ± 1.3 and 8.8 ± 1.1 for wildtype neurons, respectively, and −24.9 ± 1.5 and 9.1 ± 1.5 for *NF1*$^{+/ex42del}$ neurons, respectively. Similarly, the voltage-dependence for inactivation of Gmax was nearly identical between the two genotypes: $V_{0.5}$ and k were −6.9 ± 1.0 and 6.0 ± 0.8 for wildtype neurons, respectively, and −9.2 ± 1.6 and 4.5 ± 1.1 for *NF1*$^{+/ex42del}$ neurons, respectively. These results confirmed that calcium currents are increased in *NF1*$^{+/ex42del}$ pig DRGs compared to wildtype swine DRGs.

3.4. Changes in CRMP2 phosphorylation in NF1$^{+/ex42del}$ pig DRGs underpin the changes in calcium channel remodeling

To determine the mechanism of the increased calcium currents in *NF1*$^{+/ex42del}$ neurons, we explored the underlying signaling. In neurons, neurofibromin interacts with CRMP2 to repress its phosphorylation by cyclin dependent kinase 5 (Cdk5) on a serine residue at position 522 of CRMP2 – a site found to be important for hyperalgesia in the context of NF1 [52; 57; 60]. We have also reported that CRISPR/Cas9 mediated excision of the C-terminal domain of neurofibromin abolished the interaction with CRMP2, thus leading to increased CRMP2 phosphorylation in rodent DRG and spinal cord [58]. We asked if this effect on CRMP2 phosphorylation is recapitulated in our new *NF1* mutant miniswine model. We used phosphoproteomics to assess CRMP2 phosphorylation in pig DRGs (Figure 5A). This is an unbiased approach that enables detection of all CRMP2 phosphorylation events independently of available antibodies, many of which have not been validated in pigs (data not shown). Using mass spectrometry, we analyzed whole DRG lysates from wildtype and *NF1*$^{+/ex42del}$ pigs (n=6 each). While CRMP2 expression levels were not changed by *NF1* mutation (Figure 5A), these analyses uncovered several novel observations about the porcine protein. First, the peptide ions identified in pig DRGs mapped to a long form of CRMP2. This long form results from a splicing event on the mRNA that adds nearly 100 amino acids onto the N-terminus of the protein. Prior studies showed that this alternate CRMP2 form exists in humans [66], but it is not present in rodents. The extensive genome and transcriptome sequencing performed in the last 20 years allows us to mine experimental evidence of transcripts for any gene. In the Ensembl and Nucleotide databases, alternative transcripts leading to a long form of CRMP2 are referenced for humans with published evidence at the protein level [66].

Second, we identified 3 phosphorylation sites on CRMP2 (Serine 27, Serine 627, and Serine 647) whose modification was altered by *NF1* status (Figure 5A). In DRGs of *NF1*$^{+/ex42del}$ pigs, S27 and S647 phosphorylation levels were unchanged while the S627 phosphorylation level was increased (Figure 5A). The kinases responsible for phosphorylation at residues S27 and S647 are unknown. We used GPS 3.0 to predict the kinases (selected for a high threshold, false discovery rate <10%) that might mediate the phosphorylation of CRMP2 at these novel sites. Several potential kinases are implicated for S27 phosphorylation including those from the Dual specificity Tyrosine Regulated Kinase (DYRK), Cyclin Dependent Kinase (CDK) and Tau-Tubulin Kinase (TTBK) families but also by MAPK12 (Mitogen-activated protein kinase 12), and KIS, a kinase associated with microtubule regulators. The S647 phosphorylation site had a completely different predicted kinase landscape with candidate kinases including NIMA (never in mitosis gene a)-related kinase 2 (NEK2), LIM domain kinase 1 (LIMK1) and type 1 serine/threonine kinase receptors including activin-like receptors 1–7 (ALK1–7) were possible candidates for the phosphorylation. Serine 627 is analogous to the Cdk5 regulated S522 phosphorylation site that is present in both rodents and humans. These analyses identified two novel phosphorylation sites in CRMP2 and demonstrated that DRGS from *NF1*$^{+/ex42del}$ pigs have altered CRMP2 phosphorylation. A limitation of the proteomics approach is that we cannot conclude whether these new phosphorylation sites are neuron-specific.

3.5. Increased depolarization of evoked calcium influx in sensory neurons of NF1$^{+/ex42del}$ pigs can be reduced by (S)-lacosamide, an inhibitor of CRMP2 phosphorylation

In NF1, the expression and function of voltage-gated calcium channels is increased [58; 74]. This increase was demonstrated to be reliant on CRMP2 phosphorylation level (S522) in rodent models [58]. Since we found increased CRMP2 phosphorylation at the Cdk5 site (S627) in *NF1*$^{+/ex42del}$ pig (Figure 5A), we next asked if the CRMP2 phosphorylation inhibitor (*S*)-lacosamide ((*S*)-LCM) [53–55] could be used to reverse the increased calcium influx as we previously demonstrated in a rat model of NF1 [58]. Expressing a CRMP2 mimicking a constitutive phosphorylation abolishes all actions of (*S*)-LCM [58], supporting this small molecule as a selective inhibitor of CRMP2 phosphorylation [53; 55]. DRG cultures were generated from either wildtype or *NF1*$^{+/ex42del}$ pig DRGs and then imaged for depolarization- evoked calcium influx. We observed that *NF1*$^{+/ex42del}$ pig DRGs had an augmented calcium influx compared to wildtype pig DRGs (Figure 5B), thus replicating our previous finding in pig [74] and in rodent [58] neurons. Treatment with (*S*)-LCM decreased depolarization-evoked calcium influx in both wildtype and *NF1*$^{+/ex42del}$ pig DRGs (Figure 5C). These data demonstrate that pharmacological antagonism of CRMP2 phosphorylation can reduce the activity of voltage-gated calcium channels, setting the stage for translational studies to evaluate this small molecule in future pain behaviors in this NF1 mutant miniswine model.

3.6. Increased depolarization of evoked calcium influx in sensory neurons of NF1$^{+/ex42del}$ pigs can be reduced by inhibition of CaV2.2.

We found that the activity of the voltage gated N-type calcium channel (CaV2.2) was increased in DRG neurons from *Nf1*$^{+/-}$ mice [22; 71], CRISPR edited rat and in our *NF1*$^{+/ex42del}$ pig DRG neurons [74]. Recently, we have developed a novel approach to specifically inhibit CaV2.2 by targeting the interface between the α1B and the accessory β-subunits of the N-type calcium channel [39]. We identified the small molecule IPPQ to be able to uncouple this interaction, inhibit N-type related calcium currents and reverse thermal hyperalgesia in our rat model [58] of CRISPR-induced NF1 related pain [39]. To evaluate the therapeutic potential of IPPQ in our model of *NF1*$^{+/ex42del}$ pig, small to medium diameter DRG neurons were treated overnight with 20 μM of IPPQ and calcium currents recorded in wildtype or *NF1*$^{+/ex42del}$ DRGs (Figure 6A–B). We found that IPPQ inhibited calcium currents in both wildtype and *NF1*$^{+/ex42del}$ pig DRGs (Figure 6C–F). Similar to what we observed in rat DRG neurons, IPPQ had no effect on the activation or the inactivation properties of the voltage gated calcium channels (Figure 6G–J). These results show that the novel N-type calcium channel inhibitor IPPQ could be used to dampen the increased CaV2.2 activity in DRG sensory neurons in NF1. This observation has a high translational value and suggests that IPPQ could have the potential to reverse idiopathic pain in NF1 patients.

4. Discussion

Research spanning the last thirty years has shown that the heterogeneity of clinical manifestations of NF1 is not seen with rodent models, limiting their translational impact. Here, in this swine model, we demonstrated: (*i*) increases in calcium conductance likely

attributable to increased CRMP2 phosphorylation, a known allosteric regulator of these channels [16; 27]; (*ii*) first characterization of pain-related behaviors in a swine model which allowed identification of lowered tactile (allodynia) and thermal (hyperalgesia) thresholds in *NF1*$^{+/ex42del}$ pigs compared to their wildtype counterparts; (*iii*) disrupted sleep quality and greater rest time in *NF1*$^{+/ex42del}$ pigs; (*iv)* correlation of allodynia and quality of life measurements; and (*v*) normalization of increased calcium influx in *NF1*$^{+/ex42del}$ pig DRGs by pharmacological antagonism of CRMP2 phosphorylation or of the interaction between the α1B and the accessory β-subunits of the N-type calcium channel. Overall, the data supports the use of the *NF1*$^{+/ex42del}$ pigs as a new model for studying NF1 compared to rodents, as it is the only heterozygous model that displays spontaneous neurofibroma formation, and it allows for more similar comparisons of anatomy, physiology, and drug metabolism. Additionally, our study suggests that antagonizing CaV2.2 channel function might be a promising therapeutic strategy for NF1-related pain management.

An issue in interpreting signaling changes in mutant *NF1* miniswine is delineating the mechanism of increased calcium signaling and its possible relationship to pain. In our earlier studies with deletion of the *Nf1* gene in rodents, we had identified a signaling pathway that involved increased phosphorylation of CRMP2, a regulator of N-type CaV2.2 channels. CRMP2 bound to CaV2.2 leading to increased Ca^{2+} current density and increased neurotransmitter release in sensory neurons [16]. CRMP2 interacted with the C-terminal domain of neurofibromin [44; 60], such that deletion of neurofibromin (or the C-terminal portion) increased CRMP2 phosphorylation [60], which in turn, increased its association with CaV2.2 [9; 55]. *NF1* deletion was accompanied by an increase in sensory neuron excitability, and increased depolarization-evoked calcitonin gene-related peptide (CGRP) release in the spinal cord [52]. We determined that these dysregulations were due to the loss of CRMP2 interaction with neurofibromin, thus identifying the CRMP2-neurofibromin interface and CRMP2 phosphorylation as drivers of NF1-related pain [57; 58]. The increase in calcium currents in DRGs from *NF1*$^{+/ex42del}$ pigs is consistent with our previous report of increased calcium influx measured with calcium-dye based fluorescence methods [74] as well as with reports in mouse [22; 71] and rat [58] models of NF1. An alternative mechanism, that remains to be tested, is activation of sensory neurons through mast cell degranulation or hyperproliferation [15], which could lead to hyperexcitability.

Notably, our unbiased phosphoproteomics data bring to bear new evidence regarding the allosteric regulation of CRMP2. First, we identified a larger variant of CRMP2, which has also been found in humans [66] but absent in rodents. The porcine peptides belonging to the long form of CRMP2, sometimes described as CRMP2-A [3; 79], were detected here by mass spectrometry. This observation highlights a greater degree of similarity between pigs and humans compared to rodents, supporting the notion that pigs are superior models of the human condition than rodents. Thus, to better model a disease related to CRMP2, one needs to use an animal model expressing human-equivalent splice variants, and pigs express several splice variants for CRMP2 [79]. Thus, the *NF1*$^{+/ex42del}$ pig model is a more suitable for studying this CRMP2-related genetic disease.

Second, we found three sites of phosphorylation in CRMP2, including two previously unknown phosphorylated residues in pig CRMP2 - S27 and S627. Because these

phosphorylation sites were found from whole DRG lysates, it is unknown whether these are neuron specific events or also present in non-neuronal cells. Among these predicted kinases, increased KIS expression level was reported in NF1-associated plexiform neurofibromas and in MPNSTs [6]. ALKs are known regulators of neurofibromin function [29] and participate in learning and cognitive defect in a mouse model of NF1 [72; 73]. Therefore, CRMP2 phosphorylation by KIS or ALK may contribute to NF1 pathophysiology. Here, we identified increased CRMP2 phosphorylation by Cdk5 (S522 site in rodents, S627 in pigs from this study), which as previously demonstrated [58], contributes to NF1-related pain. We also found that the CRMP2 phosphorylation inhibitor (S)-LCM, reversed the increased calcium influx in *NF1*$^{+/ex42del}$ pig DRGs [53; 55]. This shows that the mechanism of increased voltage gated calcium channel function in NF1 involving increased CRMP2 phosphorylation by Cdk5 is translational from rodent models to our mutant pig model.

Pain in NF1 has been largely overlooked [5; 17; 76]. Between 29–70% of NF1 patients report pain [17; 26], with ~70% of children and adults with NF1 using prescription pain medications [17], and pain being reported as a key symptom of NF1 patients affecting their quality of life [17; 49; 68; 76]. Large animal models of rare diseases are important for understanding disease mechanisms and driving therapeutic discovery. However, behavioral profiling in these large, barn-housed species is challenging and not well-characterized. Typically, pain in pigs has been estimated by responses to nociceptive stimuli, using vocalization, or a composite of observed behavioral parameters such as presentation of lameness, aggression, restlessness, posture, isolation, and agitation. Other investigators have analyzed pain indicators by observing inactivity, huddling up, trembling, tail-wagging, scratching, stiffness, sleep spasms, recumbency, coprophagy, aggression, depression, head-pressing, changes in activity, nursing, lying, body movement, muscle-twitching, and withdrawal [28]. In a pig model for chronic pain caused by surgically induced peripheral neuritis trauma, Castel and colleagues [12] used von Frey filaments to assess mechanical sensitivity, a pigeon feather to asses tactile sensitivity, and a composite behaviors scale to assess spontaneous pain behaviors. We found that both female and tumor-burdened male *NF1*$^{+/ex42del}$ pigs responded to lower target forces of mechanical stimulation than their wildtype counterparts independent of agitation, suggesting presence of allodynia. The observed allodynia appeared to be ‘transient’ in nature as it was only observed in younger (i.e. 9-months-old) pigs; the reason for this is unclear but may reflect learning of the behavior and/or testing fatigue. We also observed a hyperalgesic phenotype in *NF1*$^{+/ex42del}$ pigs, when thermally stimulated, which is consistent with hyperalgesia noted in mice haploinsufficient for *Nf1* [48]. Remarkably, this hyperalgesic behavior was observed only in female pigs, suggesting a sexual dimorphism in pain in NF1. Importantly, however, we found that responses to these assays diminished over time, indicating the importance of intermittent testing in this animal model to reduce testing fatigue.

Fragmented sleep was reported in *Nf1*^{cKO} mutant mice [1] and poor sleep quality is a life quality-affecting symptom of NF1 patients [43; 47] and highly associated comorbidity of pain [2]. As pain and sleep deficits are also observed in NF1 patients [26], it is remarkable that *NF1*$^{+/ex42del}$ female and tumor-burdened male pigs exhibit increased rest time and depreciated sleep quality in comparison to their wildtype counterparts. Importantly, these quality of life measures correlate strongly with von Frey allodynia measurements, with

tumor-burdened animals clustering at high scores on all assays, indicating that these pain comorbidities may be related to the presence of tumors in the *NF1*$^{+/ex42del}$ pigs. However, there are limitations to our work, as the number of animals with tumors was limited, and future work must focus on delineating the presence, location, and size of tumors on allodynia and quality of life measurements. Female *NF1*$^{+/ex42del}$ animals also scored poorly on FitBark quality of life measures, though at the time of the study there were no wildtype female animals available as a comparison. As sleep cycles can be influenced due to differing hormones across sexes or age, future studies must confirm sleep disturbances in female animals when compared to proper controls [10; 65]. Additionally, to date, no female *NF1*$^{+/ex42del}$ animals have developed tumors, so we cannot conclude the role of gender and tumor-specific phenotypic differences on pain comorbidities in health-related quality of life domains. We previously noted that female animals had yet to form tumors [74], and the current study has monitored these animals up to 24 months of age. It is unclear why female *NF1*$^{+/ex42del}$ animals do not form tumors (but see [21]).

From a clinical perspective, pain is comorbid with symptoms in many health-related quality-of-life domains. Even with regard to the general, non-NF1 population, pain has often been seen in conjunction specifically with depreciated sleep quality. For example, in approaching therapies for chronic spinal pain, Malfliet and colleagues also addressed comorbid insomnia [46]. Song and colleagues highlighted the correlation between migraine and poor sleep quality [64]. In fact, ~48% of the 2695 participants with reported migraines also exhibited poor sleep quality. Along these lines, pain is comorbid with sleep deficits in the NF1 patient population as well. Fjermestad and colleagues reported that in NF1 patients, there is a positive correlation between pain and sleep problems (0.48) [26]. Our miniswine model of NF1 phenocopies this comorbidity of NF1 pain, allowing us to employ a biopsychosocial approach to NF1 pain research that, to our knowledge, is not possible in any rodent model.

In summary, this work characterizes a transgenic miniswine model of NF1 pain. We established several different measures for nociceptive dysregulation such as CRMP2 phosphorylation, voltage gated calcium channel regulation, pain related behaviors, and quality of life-related health measures. Besides providing new insights into mechanisms of NF1 nociception, this pig model of NF1 also captures comorbid symptoms of NF1 pain such as sleep deficits that are not seen in rodent models.

Supplementary Material

Refer to Web version on PubMed Central for supplementary material.

Acknowledgements –

This work was supported by National Institutes of Health Awards (1R01NS098772, 1R01DA042852, and R01AT009716 to RK); a Neurofibromatosis New Investigator Award from the Department of Defense Congressionally Directed Military Medical Research and Development Program (NF1000099 to RK); and funding from the Synodos for NF1 program at the Children's Tumor Foundation to DKM, BWD, CSR, JCS, DEQ, and JMW; a research award from the Children's Tumor Foundation (2015-04-009A) to RK and JMW; a Children's Tumor Foundation NF1 Synodos award to R.K. A.M. was supported by a Young Investigator's Award from the Children's Tumor Foundation. SSB was supported by funds to the University of Arizona's Undergraduate Biology Research Program. The authors would like to thank Trisha Smit, Brian Dacken, and Justin Van Kalsbeek of Exemplar Genetics, Iowa, USA for their assistance in swine behavior testing and management and Dr. Paul

Langlais and Natalie Barker from the proteomics lab, college of medicine at the University of Arizona for their training and assistance in performing the mass spectrometry experiment.

References

[1]. Anastasaki C, Rensing N, Johnson KJ, Wong M, Gutmann DH. Neurofibromatosis type 1 (Nf1)-mutant mice exhibit increased sleep fragmentation. J Sleep Res 2019:e12816. [PubMed: 30609083]

[2]. Axen I Pain-related Sleep Disturbance: A Prospective Study With Repeated Measures. The Clinical journal of pain 2016;32(3):254–259. [PubMed: 25968449]

[3]. Balastik M, Zhou XZ, Alberich-Jorda M, Weissova R, Ziak J, Pazyra-Murphy MF, Cosker KE, Machonova O, Kozmikova I, Chen CH, Pastorino L, Asara JM, Cole A, Sutherland C, Segal RA, Lu KP. Prolyl Isomerase Pin1 Regulates Axon Guidance by Stabilizing CRMP2A Selectively in Distal Axons. Cell Rep 2015;13(4):812–828. [PubMed: 26489457]

[4]. Ballester R, Marchuk D, Boguski M, Saulino A, Letcher R, Wigler M, Collins F. The NF1 locus encodes a protein functionally related to mammalian GAP and yeast IRA proteins. Cell 1990;63(4):851–859. [PubMed: 2121371]

[5]. Bellampalli SS, Khanna R. Towards a neurobiological understanding of pain in neurofibromatosis type 1: mechanisms and implications for treatment. Pain 2019;160(5):1007–1018. [PubMed: 31009417]

[6]. Bieche I, Manceau V, Curmi PA, Laurendeau I, Lachkar S, Leroy K, Vidaud D, Sobel A, Maucuer A. Quantitative RT-PCR reveals a ubiquitous but preferentially neural expression of the KIS gene in rat and human. Brain Res Mol Brain Res 2003;114(1):55–64. [PubMed: 12782393]

[7]. Brannan CI, Perkins AS, Vogel KS, Ratner N, Nordlund ML, Reid SW, Buchberg AM, Jenkins NA, Parada LF, Copeland NG. Targeted disruption of the neurofibromatosis type-1 gene leads to developmental abnormalities in heart and various neural crest-derived tissues. Genes & development 1994;8(9):1019–1029. [PubMed: 7926784]

[8]. Brittain JM, Duarte DB, Wilson SM, Zhu W, Ballard C, Johnson PL, Liu N, Xiong W, Ripsch MS, Wang Y, Fehrenbacher JC, Fitz SD, Khanna M, Park CK, Schmutzler BS, Cheon BM, Due MR, Brustovetsky T, Ashpole NM, Hudmon A, Meroueh SO, Hingtgen CM, Brustovetsky N, Ji RR, Hurley JH, Jin X, Shekhar A, Xu XM, Oxford GS, Vasko MR, White FA, Khanna R. Suppression of inflammatory and neuropathic pain by uncoupling CRMP-2 from the presynaptic Ca(2)(+) channel complex. Nature medicine 2011;17(7):822–829.

[9]. Brittain JM, Wang Y, Eruvwetere O, Khanna R. Cdk5-mediated phosphorylation of CRMP-2 enhances its interaction with CaV2.2. FEBS letters 2012;586(21):3813–3818. [PubMed: 23022559]

[10]. Carrier J, Semba K, Deurveilher S, Drogos L, Cyr-Cronier J, Lord C, Sekerovick Z. Sex differences in age-related changes in the sleep-wake cycle. Front Neuroendocrinol 2017;47:66–85. [PubMed: 28757114]

[11]. Castel D, Naveh M, Aharon A, Doron O, Meilin S. Prolonged Analgesic Effect of PRF-108 and PRF-110 on Post-operative Pain in Pigs. Pain Ther 2016;5(1):29–42. [PubMed: 26724813]

[12]. Castel D, Willentz E, Doron O, Brenner O, Meilin S. Characterization of a porcine model of post-operative pain. Eur J Pain 2014;18(4):496–505. [PubMed: 24105754]

[13]. Cawthon RM, O'Connell P, Buchberg AM, Viskochil D, Weiss RB, Culver M, Stevens J, Jenkins NA, Copeland NG, White R. Identification and characterization of transcripts from the neurofibromatosis 1 region: the sequence and genomic structure of EVI2 and mapping of other transcripts. Genomics 1990;7(4):555–565. [PubMed: 2117566]

[14]. Chambers MC, Maclean B, Burke R, Amodei D, Ruderman DL, Neumann S, Gatto L, Fischer B, Pratt B, Egertson J, Hoff K, Kessner D, Tasman N, Shulman N, Frewen B, Baker TA, Brusniak MY, Paulse C, Creasy D, Flashner L, Kani K, Moulding C, Seymour SL, Nuwaysir LM, Lefebvre B, Kuhlmann F, Roark J, Rainer P, Detlev S, Hemenway T, Huhmer A, Langridge J, Connolly B, Chadick T, Holly K, Eckels J, Deutsch EW, Moritz RL, Katz JE, Agus DB, MacCoss M, Tabb DL, Mallick P. A cross-platform toolkit for mass spectrometry and proteomics. Nat Biotechnol 2012;30(10):918–920. [PubMed: 23051804]

[15]. Chatterjea D, Martinov T. Mast cells: versatile gatekeepers of pain. Mol Immunol 2015;63(1):38–44. [PubMed: 24666768]

[16]. Chi XX, Schmutzler BS, Brittain JM, Hingtgen CM, Nicol GD, Khanna R. Regulation of N-type voltage-gated calcium (CaV2.2) channels and transmitter release by collapsin response mediator protein-2 (CRMP-2) in sensory neurons. JCell Sci 2009;23:4351–4362.

[17]. Creange A, Zeller J, Rostaing-Rigattieri S, Brugieres P, Degos JD, Revuz J, Wolkenstein P. Neurological complications of neurofibromatosis type 1 in adulthood. Brain 1999;122(Pt 3):473–481. [PubMed: 10094256]

[18]. Dasgupta B, Yi Y, Chen DY, Weber JD, Gutmann DH. Proteomic analysis reveals hyperactivation of the mammalian target of rapamycin pathway in neurofibromatosis 1-associated human and mouse brain tumors. Cancer Res 2005;65(7):2755–2760. [PubMed: 15805275]

[19]. Daston MM, Ratner N. Neurofibromin, a predominantly neuronal GTPase activating protein in the adult, is ubiquitously expressed during development. Dev Dyn 1992;195(3):216–226. [PubMed: 1301085]

[20]. Daston MM, Scrable H, Nordlund M, Sturbaum AK, Nissen LM, Ratner N. The protein product of the neurofibromatosis type 1 gene is expressed at highest abundance in neurons, Schwann cells, and oligodendrocytes. Neuron 1992;8(3):415–428. [PubMed: 1550670]

[21]. Dischinger PS, Tovar EA, Essenburg CJ, Madaj ZB, Gardner EE, Callaghan ME, Turner AN, Challa AK, Kempston T, Eagleson B, Kesterson RA, Bronson RT, Bowman MJ, Graveel CR, Steensma MR. NF1 deficiency correlates with estrogen receptor signaling and diminished survival in breast cancer. NPJ Breast Cancer 2018;4:29. [PubMed: 30182054]

[22]. Duan JH, Hodgdon KE, Hingtgen CM, Nicol GD. N-type calcium current, Cav2.2, is enhanced in small-diameter sensory neurons isolated from Nf1+/− mice. Neuroscience 2014;270:192–202. [PubMed: 24755485]

[23]. Dustrude ET, Wilson SM, Ju W, Xiao Y, Khanna R. CRMP2 protein SUMOylation modulates NaV1.7 channel trafficking. The Journal of biological chemistry 2013;288(34):24316–24331. [PubMed: 23836888]

[24]. Evans DG, O'Hara C, Wilding A, Ingham SL, Howard E, Dawson J, Moran A, Scott-Kitching V, Holt F, Huson SM. Mortality in neurofibromatosis 1: in North West England: an assessment of actuarial survival in a region of the UK since 1989. European journal of human genetics : EJHG 2011;19(11):1187–1191. [PubMed: 21694737]

[25]. Field MJ, Cox PJ, Stott E, Melrose H, Offord J, Su TZ, Bramwell S, Corradini L, England S, Winks J, Kinloch RA, Hendrich J, Dolphin AC, Webb T, Williams D. Identification of the alpha2-delta-1 subunit of voltage-dependent calcium channels as a molecular target for pain mediating the analgesic actions of pregabalin. Proceedings of the National Academy of Sciences of the United States of America 2006;103(46):17537–17542. [PubMed: 17088553]

[26]. Fjermestad KW, Nyhus L, Kanavin OJ, Heiberg A, Hoxmark LB. Health Survey of Adults with Neurofibromatosis 1 Compared to Population Study Controls. J Genet Couns 2018.

[27]. Francois-Moutal L, Wang Y, Moutal A, Cottier KE, Melemedjian OK, Yang X, Wang Y, Ju W, Largent-Milnes TM, Khanna M, Vanderah TW, Khanna R. A membrane-delimited N-myristoylated CRMP2 peptide aptamer inhibits CaV2.2 trafficking and reverses inflammatory and postoperative pain behaviors. Pain 2015;156(7):1247–1264. [PubMed: 25782368]

[28]. Gigliuto C, De Gregori M, Malafoglia V, Raffaeli W, Compagnone C, Visai L, Petrini P, Avanzini MA, Muscoli C, Vigano J, Calabrese F, Dominioni T, Allegri M, Cobianchi L. Pain assessment in animal models: do we need further studies? J Pain Res 2014;7:227–236. [PubMed: 24855386]

[29]. Gouzi JY, Moressis A, Walker JA, Apostolopoulou AA, Palmer RH, Bernards A, Skoulakis EM. The receptor tyrosine kinase Alk controls neurofibromin functions in Drosophila growth and learning. PLoS Genet 2011;7(9):e1002281. [PubMed: 21949657]

[30]. Gutmann DH, Ferner RE, Listernick RH, Korf BR, Wolters PL, Johnson KJ. Neurofibromatosis type 1. Nat Rev Dis Primers 2017;3:17004. [PubMed: 28230061]

[31]. Gutmann DH, Rasmussen SA, Wolkenstein P, MacCollin MM, Guha A, Inskip PD, North KN, Poyhonen M, Birch PH, Friedman JM. Gliomas presenting after age 10 in individuals with neurofibromatosis type 1 (NF1). Neurology 2002;59(5):759–761. [PubMed: 12221173]

[32]. Herskin MS, Ladewig J, Arendt-Nielsen L. Measuring cutaneous thermal nociception in group-housed pigs using laser technique-effects of laser power output. Applied Animal Behaviour Science 2009;118:144–151.

[33]. Hirbe AC, Gutmann DH. Neurofibromatosis type 1: a multidisciplinary approach to care. Lancet Neurol 2014;13(8):834–843. [PubMed: 25030515]

[34]. Hyman SL, Shores A, North KN. The nature and frequency of cognitive deficits in children with neurofibromatosis type 1. Neurology 2005;65(7):1037–1044. [PubMed: 16217056]

[35]. Ibrahim MM, Patwardhan A, Gilbraith KB, Moutal A, Yang X, Chew LA, Largent-Milnes T, Malan TP, Vanderah TW, Porreca F, Khanna R. Long-lasting antinociceptive effects of green light in acute and chronic pain in rats. Pain 2017;158(2):347–360. [PubMed: 28092651]

[36]. Isakson SH, Rizzardi AE, Coutts AW, Carlson DF, Kirstein MN, Fisher J, Vitte J, Williams KB, Pluhar GE, Dahiya S, Widemann BC, Dombi E, Rizvi T, Ratner N, Messiaen L, Stemmer-Rachamimov AO, Fahrenkrug SC, Gutmann DH, Giovannini M, Moertel CL, Largaespada DA, Watson AL. Genetically engineered minipigs model the major clinical features of human neurofibromatosis type 1. Commun Biol 2018;1:158. [PubMed: 30302402]

[37]. Jacks T, Shih TS, Schmitt EM, Bronson RT, Bernards A, Weinberg RA. Tumour predisposition in mice heterozygous for a targeted mutation in Nf1. Nat Genet 1994;7(3):353–361. [PubMed: 7920653]

[38]. Kaiser EA, Kuburas A, Recober A, Russo AF. Modulation of CGRP-induced light aversion in wild-type mice by a 5-HT(1B/D) agonist. The Journal of neuroscience : the official journal of the Society for Neuroscience 2012;32(44):15439–15449. [PubMed: 23115181]

[39]. Khanna R, Yu J, Yang X, Moutal A, Chefdeville A, Gokhale V, Shuja Z, Chew LA, Bellampalli SS, Luo S, Francois-Moutal L, Serafini MJ, Ha T, Perez-Miller S, Park KD, Patwardhan AM, Streicher JM, Colecraft HM, Khanna M. Targeting the CaValpha-CaVbeta interaction yields an antagonist of the N-type CaV2.2 channel with broad antinociceptive efficacy. Pain 2019.

[40]. Kongkriangkai AM, King C, Martin LJ, Wakefield E, Prada CE, Kelly-Mancuso G, Schorry EK. Substantial pain burden in frequency, intensity, interference and chronicity among children and adults with neurofibromatosis Type 1. Am J Med Genet A 2019;179(4):602–607. [PubMed: 30737893]

[41]. Krzyzanowska A, Avendano C. Behavioral testing in rodent models of orofacial neuropathic and inflammatory pain. Brain Behav 2012;2(5):678–697. [PubMed: 23139912]

[42]. Kwon CH, Zhao D, Chen J, Alcantara S, Li Y, Burns DK, Mason RP, Lee EY, Wu H, Parada LF. Pten haploinsufficiency accelerates formation of high-grade astrocytomas. Cancer Res 2008;68(9):3286–3294. [PubMed: 18451155]

[43]. Leschziner GD, Golding JF, Ferner RE. Sleep disturbance as part of the neurofibromatosis type 1 phenotype in adults. American journal of medical genetics Part A 2013;161(6):1319–1322.

[44]. Lin YL, Hsueh YP. Neurofibromin interacts with CRMP-2 and CRMP-4 in rat brain. Biochemical and biophysical research communications 2008;369(2):747–752. [PubMed: 18313395]

[45]. Listernick R, Louis DN, Packer RJ, Gutmann DH. Optic pathway gliomas in children with neurofibromatosis 1: consensus statement from the NF1 Optic Pathway Glioma Task Force. Annals of neurology 1997;41(2):143–149. [PubMed: 9029062]

[46]. Malfliet A, Bilterys T, Van Looveren E, Meeus M, Danneels L, Ickmans K, Cagnie B, Mairesse O, Neu D, Moens M, Goubert D, Kamper SJ, Nijs J. The added value of cognitive behavioral therapy for insomnia to current best evidence physical therapy for chronic spinal pain: protocol of a randomized controlled clinical trial. Brazilian journal of physical therapy 2018.

[47]. Marana Perez AI, Duat Rodriguez A, Soto Insuga V, Dominguez Carral J, Puertas Martin V, Gonzalez Gutierrez Solana L. Prevalence of sleep disorders in patients with neurofibromatosis type 1. Neurologia 2015;30(9):561–565. [PubMed: 24975344]

[48]. Marquez de PB, Hammond DL. Sex dependent enhancement of pain responses in a mouse model of neurofibromatosis., Proceedings of the Society for Neuroscience, 2011.

[49]. Martin S, Gillespie A, Wolters PL, Widemann BC. Experiences of families with a child, adolescent, or young adult with neurofibromatosis type 1 and plexiform neurofibroma evaluated

for clinical trials participation at the National Cancer Institute. Contemp Clin Trials 2011;32(1): 10–15. [PubMed: 20951236]

[50]. Meyerholz DK, Reznikov LR. Simple and reproducible approaches for the collection of select porcine ganglia. Journal of neuroscience methods 2017;289:93–98. [PubMed: 28602889]

[51]. Mills C, Leblond D, Joshi S, Zhu C, Hsieh G, Jacobson P, Meyer M, Decker M. Estimating efficacy and drug ED50's using von Frey thresholds: impact of weber's law and log transformation. The journal of pain : official journal of the American Pain Society 2012;13(6): 519–523. [PubMed: 22543045]

[52]. Moutal A, Cai S, Luo S, Voisin R, Khanna R. CRMP2 is necessary for Neurofibromatosis type 1 related pain. Channels (Austin) 2018;12(1):47–50. [PubMed: 28837387]

[53]. Moutal A, Chew LA, Yang X, Wang Y, Yeon SK, Telemi E, Meroueh S, Park KD, Shrinivasan R, Gilbraith KB, Qu C, Xie JY, Patwardhan A, Vanderah TW, Khanna M, Porreca F, Khanna R. (S)-lacosamide inhibition of CRMP2 phosphorylation reduces postoperative and neuropathic pain behaviors through distinct classes of sensory neurons identified by constellation pharmacology. Pain 2016;157(7):1448–1463. [PubMed: 26967696]

[54]. Moutal A, Eyde N, Telemi E, Park KD, Xie JY, Dodick DW, Porreca F, Khanna R. Efficacy of (S)-Lacosamide in preclinical models of cephalic pain. Pain Rep 2016;1(1):1–10.

[55]. Moutal A, Francois-Moutal L, Perez-Miller S, Cottier K, Chew LA, Yeon SK, Dai J, Park KD, Khanna M, Khanna R. (S)-Lacosamide Binding to Collapsin Response Mediator Protein 2 (CRMP2) Regulates CaV2.2 Activity by Subverting Its Phosphorylation by Cdk5. Molecular neurobiology 2016;53(3):1959–1976. [PubMed: 25846820]

[56]. Moutal A, Li W, Wang Y, Ju W, Luo S, Cai S, Francois-Moutal L, Perez-Miller S, Hu J, Dustrude ET, Vanderah TW, Gokhale V, Khanna M, Khanna R. Homology-guided mutational analysis reveals the functional requirements for antinociceptive specificity of collapsin response mediator protein 2-derived peptides. British journal of pharmacology 2017.

[57]. Moutal A, Sun L, Yang X, Li W, Cai S, Luo S, Khanna R. CRMP2-Neurofibromin Interface Drives NF1-related Pain. Neuroscience 2018;381:79–90. [PubMed: 29655575]

[58]. Moutal A, Yang X, Li W, Gilbraith KB, Luo S, Cai S, Francois-Moutal L, Chew LA, Yeon SK, Bellampalli SS, Qu C, Xie JY, Ibrahim MM, Khanna M, Park KD, Porreca F, Khanna R. CRISPR/Cas9 editing of Nf1 gene identifies CRMP2 as a therapeutic target in neurofibromatosis type 1-related pain that is reversed by (S)-Lacosamide. Pain 2017;158(12):2301–2319. [PubMed: 28809766]

[59]. Newell K, Chitty J, Henson FM. "Patient reported outcomes" following experimental surgery-using telemetry to assess movement in experimental ovine models. J Orthop Res 2018;36(5): 1498–1507. [PubMed: 29087600]

[60]. Patrakitkomjorn S, Kobayashi D, Morikawa T, Wilson MM, Tsubota N, Irie A, Ozawa T, Aoki M, Arimura N, Kaibuchi K, Saya H, Araki N. Neurofibromatosis type 1 (NF1) tumor suppressor, neurofibromin, regulates the neuronal differentiation of PC12 cells via its associating protein, CRMP-2. The Journal of biological chemistry 2008;283(14):9399–9413. [PubMed: 18218617]

[61]. Rasmussen SA, Yang Q, Friedman JM. Mortality in neurofibromatosis 1: an analysis using U.S. death certificates. Am J Hum Genet 2001;68(5):1110–1118. [PubMed: 11283797]

[62]. Rice FL, Castel D, Ruggiero E, Dockum M, Houk G, Sabbag I, Albrecht PJ, Meilin S. Human-like cutaneous neuropathologies associated with a porcine model of peripheral neuritis: A translational platform for neuropathic pain. Neurobiology of Pain 2019;5.

[63]. Silva AJ, Frankland PW, Marowitz Z, Friedman E, Laszlo GS, Cioffi D, Jacks T, Bourtchuladze R. A mouse model for the learning and memory deficits associated with neurofibromatosis type I. Nature genetics 1997;15(3):281–284. [PubMed: 9054942]

[64]. Song TJ, Cho SJ, Kim WJ, Yang KI, Yun CH, Chu MK. Poor sleep quality in migraine and probable migraine: a population study. J Headache Pain 2018;19(1):58. [PubMed: 30046921]

[65]. Sorwell KG, Urbanski HF. Causes and consequences of age-related steroid hormone changes: insights gained from nonhuman primates. J Neuroendocrinol 2013;25(11):1062–1069. [PubMed: 23796387]

[66]. Tobe BTD, Crain AM, Winquist AM, Calabrese B, Makihara H, Zhao WN, Lalonde J, Nakamura H, Konopaske G, Sidor M, Pernia CD, Yamashita N, Wada M, Inoue Y, Nakamura F, Sheridan

SD, Logan RW, Brandel M, Wu D, Hunsberger J, Dorsett L, Duerr C, Basa RCB, McCarthy MJ, Udeshi ND, Mertins P, Carr SA, Rouleau GA, Mastrangelo L, Li J, Gutierrez GJ, Brill LM, Venizelos N, Chen G, Nye JS, Manji H, Price JH, McClung CA, Akiskal HS, Alda M, Chuang DM, Coyle JT, Liu Y, Teng YD, Ohshima T, Mikoshiba K, Sidman RL, Halpain S, Haggarty SJ, Goshima Y, Snyder EY. Probing the lithium-response pathway in hiPSCs implicates the phosphoregulatory set-point for a cytoskeletal modulator in bipolar pathogenesis. Proceedings of the National Academy of Sciences of the United States of America 2017;114(22):E4462–E4471. [PubMed: 28500272]

[67]. Tong J, Hannan F, Zhu Y, Bernards A, Zhong Y. Neurofibromin regulates G protein-stimulated adenylyl cyclase activity. Nature neuroscience 2002;5(2):95–96. [PubMed: 11788835]

[68]. Varni JW, Nutakki K, Swigonski NL. Pain, skin sensations symptoms, and cognitive functioning predictors of health-related quality of life in pediatric patients with Neurofibromatosis Type 1. Quality of life research : an international journal of quality of life aspects of treatment, care and rehabilitation 2018.

[69]. Viskochil D, Buchberg AM, Xu G, Cawthon RM, Stevens J, Wolff RK, Culver M, Carey JC, Copeland NG, Jenkins NA, et al. Deletions and a translocation interrupt a cloned gene at the neurofibromatosis type 1 locus. Cell 1990;62(1):187–192. [PubMed: 1694727]

[70]. Wallace MR, Marchuk DA, Andersen LB, Letcher R, Odeh HM, Saulino AM, Fountain JW, Brereton A, Nicholson J, Mitchell AL, et al. Type 1 neurofibromatosis gene: identification of a large transcript disrupted in three NF1 patients. Science 1990;249(4965):181–186. [PubMed: 2134734]

[71]. Wang Y, Brittain JM, Wilson SM, Hingtgen CM, Khanna R. Altered calcium currents and axonal growth in Nf1 haploinsufficient mice. Translational neuroscience 2010;1(2):106–114. [PubMed: 21949590]

[72]. Weiss JB, Weber S, Marzulla T, Raber J. Pharmacological inhibition of Anaplastic Lymphoma Kinase rescues spatial memory impairments in Neurofibromatosis 1 mutant mice. Behav Brain Res 2017;332:337–342. [PubMed: 28629962]

[73]. Weiss JB, Weber SJ, Torres ERS, Marzulla T, Raber J. Genetic inhibition of Anaplastic Lymphoma Kinase rescues cognitive impairments in Neurofibromatosis 1 mutant mice. Behav Brain Res 2017;321:148–156. [PubMed: 28057529]

[74]. White KA, Swier VJ, Cain JT, Kohlmeyer JL, Meyerholz DK, Tanas MR, Uthoff J, Hammond E, Li H, Rohret FA, Goeken A, Chan CH, Leidinger MR, Umesalma S, Wallace MR, Dodd RD, Panzer K, Tang AH, Darbro BW, Moutal A, Cai S, Li W, Bellampalli SS, Khanna R, Rogers CS, Sieren JC, Quelle DE, Weimer JM. A porcine model of neurofibromatosis type 1 that mimics the human disease. JCI Insight 2018;3(12).

[75]. White S, Marquez de Prado B, Russo AF, Hammond DL. Heat hyperalgesia and mechanical hypersensitivity induced by calcitonin gene-related peptide in a mouse model of neurofibromatosis. PloS one 2014;9(9):e106767. [PubMed: 25184332]

[76]. Wolkenstein P, Zeller J, Revuz J, Ecosse E, Leplege A. Quality-of-life impairment in neurofibromatosis type 1: a cross-sectional study of 128 cases. Arch Dermatol 2001;137(11): 1421–1425. [PubMed: 11708944]

[77]. Wu J, Williams JP, Rizvi TA, Kordich JJ, Witte D, Meijer D, Stemmer-Rachamimov AO, Cancelas JA, Ratner N. Plexiform and dermal neurofibromas and pigmentation are caused by Nf1 loss in desert hedgehog-expressing cells. Cancer Cell 2008;13(2):105–116. [PubMed: 18242511]

[78]. Xu GF, O'Connell P, Viskochil D, Cawthon R, Robertson M, Culver M, Dunn D, Stevens J, Gesteland R, White R, et al. The neurofibromatosis type 1 gene encodes a protein related to GAP. Cell 1990;62(3):599–608. [PubMed: 2116237]

[79]. Yuasa-Kawada J, Suzuki R, Kano F, Ohkawara T, Murata M, Noda M. Axonal morphogenesis controlled by antagonistic roles of two CRMP subtypes in microtubule organization. The European journal of neuroscience 2003;17(11):2329–2343. [PubMed: 12814366]

[80]. Zhu Y, Guignard F, Zhao D, Liu L, Burns DK, Mason RP, Messing A, Parada LF. Early inactivation of p53 tumor suppressor gene cooperating with NF1 loss induces malignant astrocytoma. Cancer Cell 2005;8(2):119–130. [PubMed: 16098465]

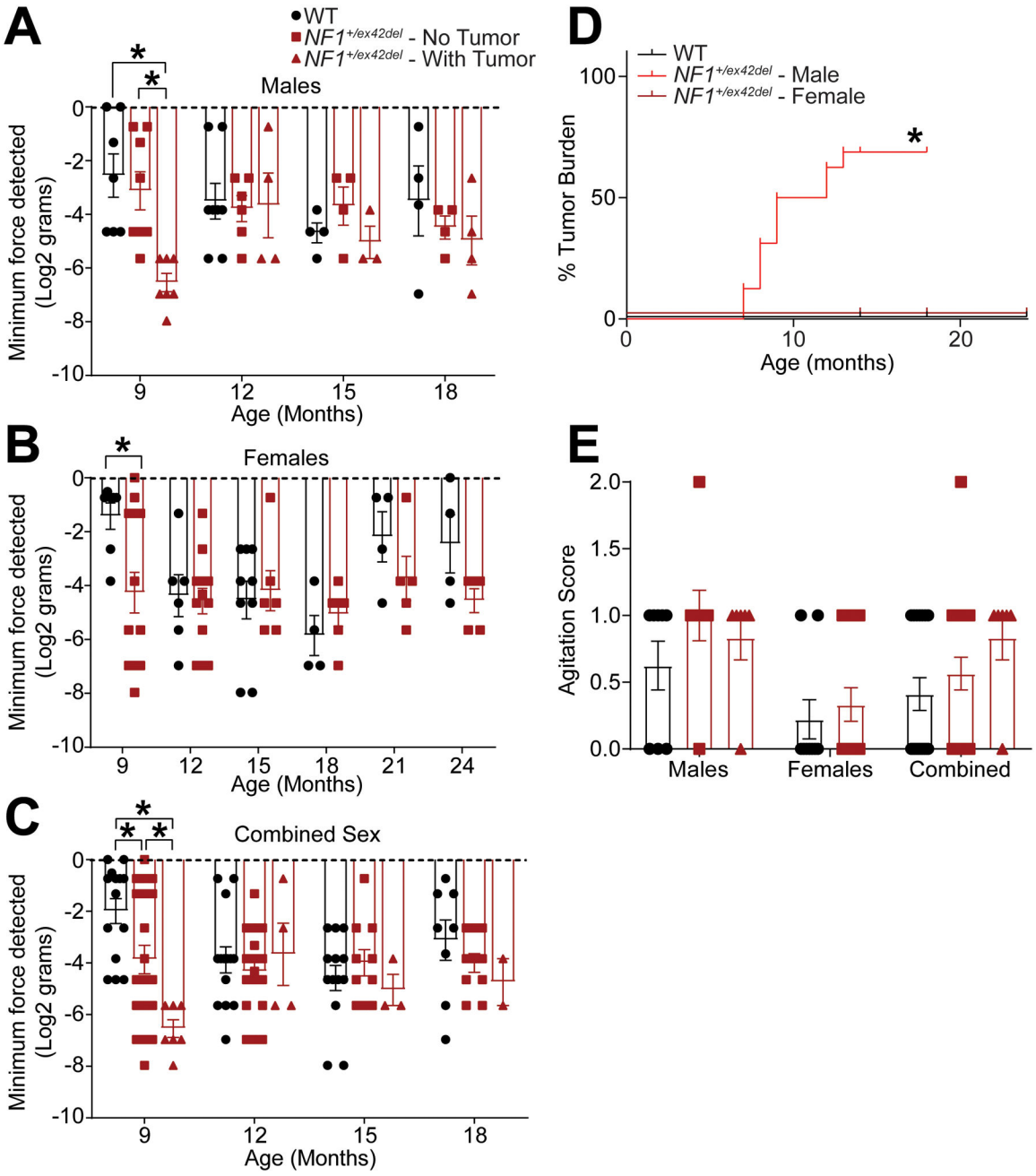

Figure 1. ***NF1*$^{+/ex42del}$ pigs exhibit transient mechanical allodynia, dependent on tumor burden and sex.**

Bar graph with scatter plot of inner ear tactile threshold values for male (**A**) or female (**B**) pigs (data is combined in (**C**)) from the indicated genotype. Tactile thresholds were decreased in both tumor-burdened male and female *NF1*$^{+/ex42del}$ pig (*p<0.05; Two-way ANOVA with Tukey post-hoc.). (**D**) Demonstration of tumor burden, showing the only male *NF1*$^{+/ex42del}$ pig exhibit tumor formation. (Mantel-Cox test, ****p<0.0001. N=16 WT, 16 NF1 males, 16 NF1 females). (**E**) Observed agitation scores as measured in Supplemental Table 2 were not significantly different between the genotypes (p>0.05, Mann Whitney), indicating anxiety or hyperactivity did not confound von Frey results in A-C.

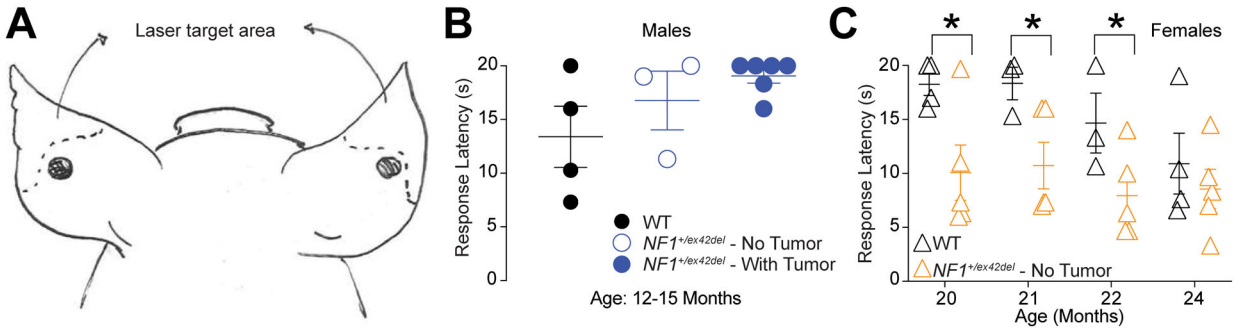

Figure 2. *NF1*$^{+/ex42del}$ pigs show sexually dimorphic behaviors in response to thermal laser stimulation.

(A) Schematic of site of thermal laser stimulation in pigs. **(B)** Male *NF1*$^{+/ex42del}$ pigs do not have enhanced response latency to thermal laser stimulation in comparison to wildtype pigs regardless of tumor presence at 12–15 months of age. **(C)** Female *NF1*$^{+/ex42del}$ pigs exhibit significantly reduced response latencies to thermal laser stimulation in comparison to wildtype pigs at several time points. Wildtype females become more sensitive to the laser stimuli over multiple testings, indicating perhaps testing fatigue and sensitization. (*$p<0.05$, ordinary two-way ANOVA, Fisher's LSD test for each time point).

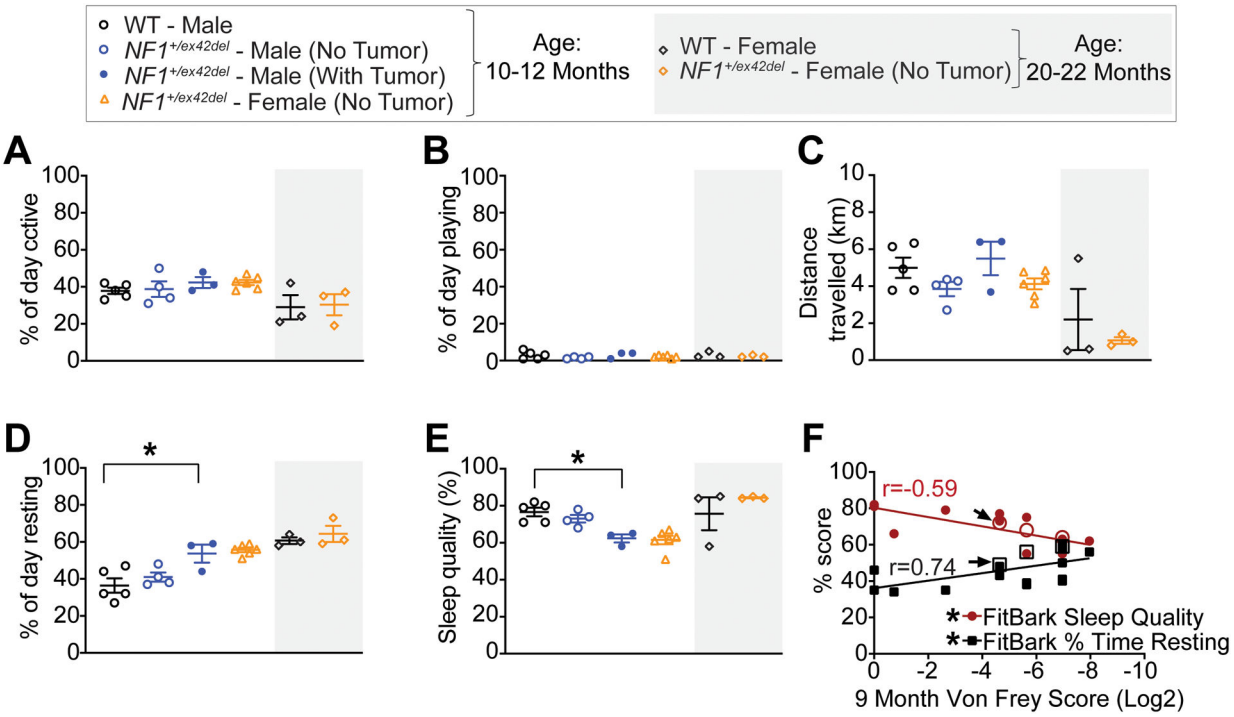

Figure 3. *NF1*$^{+/ex42del}$ pigs exhibit poor sleep and increased time resting.

Scatter plots for **(A)** percent of day active, **(B)** percent of day playing, **(C)** total distance travelled, **(D)** percent of day resting, and **(E)** sleep quality for the indicated genotype and gender at 10–12 months or 20–22 months of age. Measures of both percent of day resting and sleep quality were affected in female and tumor-burdened male *NF1*$^{+/ex42del}$ pigs. Asterisks indicate significance between compared groups (*p<0.05; One-way ANOVA with Tukey post-hoc). (**F**). Correlation analysis between 9 month von Frey data and 10–12 month FitBark quality of life data indicates significant correlation (Pearson correlation coefficient values are indicated) between the two assays. Higher sensitivity to von Frey stimuli is associated with increased rest time and decreased quality of sleep (*p<0.05). Animals with tumor burden (open circles and squares) cluster towards higher scores on all three assays. One animal appeared to be transitioning to tumor formation during testing (arrows). As this animal scored lower than the animals with established tumors, it's possible that tumor burden directly affects assay scores.

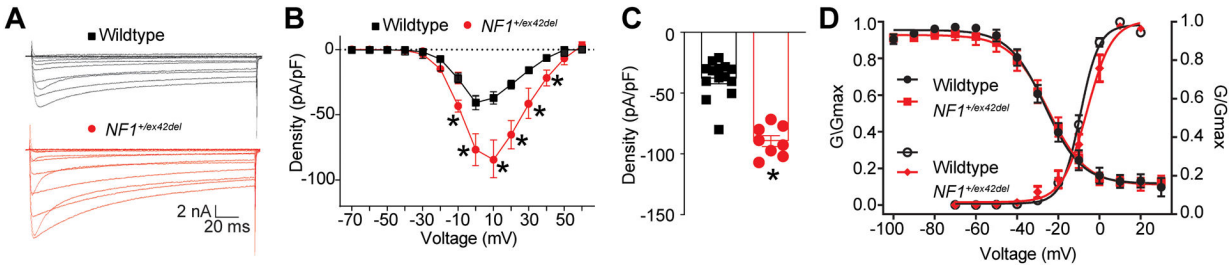

Figure 4. Calcium currents are increased in *NF1*$^{+/ex42del}$ pig DRGs.

(**A**) representative calcium traces from wildtype or *NF1*$^{+/ex42del}$ pig DRGs. (**B**) Summary current-voltage curve of peak current density normalized to the cell capacitance (pA/pF) for each voltage step. (**C**) Bar graph with scatter plot of peak current density at 10 mV for the indicated conditions. (**D**) Activation and inactivation curves of normalized calcium currents (G/Gmax) for the indicated genotype. *p<0.05, One-way ANOVA with Tukey post-hoc test, n= 8–14 cells per condition from three wildtype and two *NF1*$^{+/ex42del}$ boars. Unless otherwise stated, all data are presented as means ± SEM.

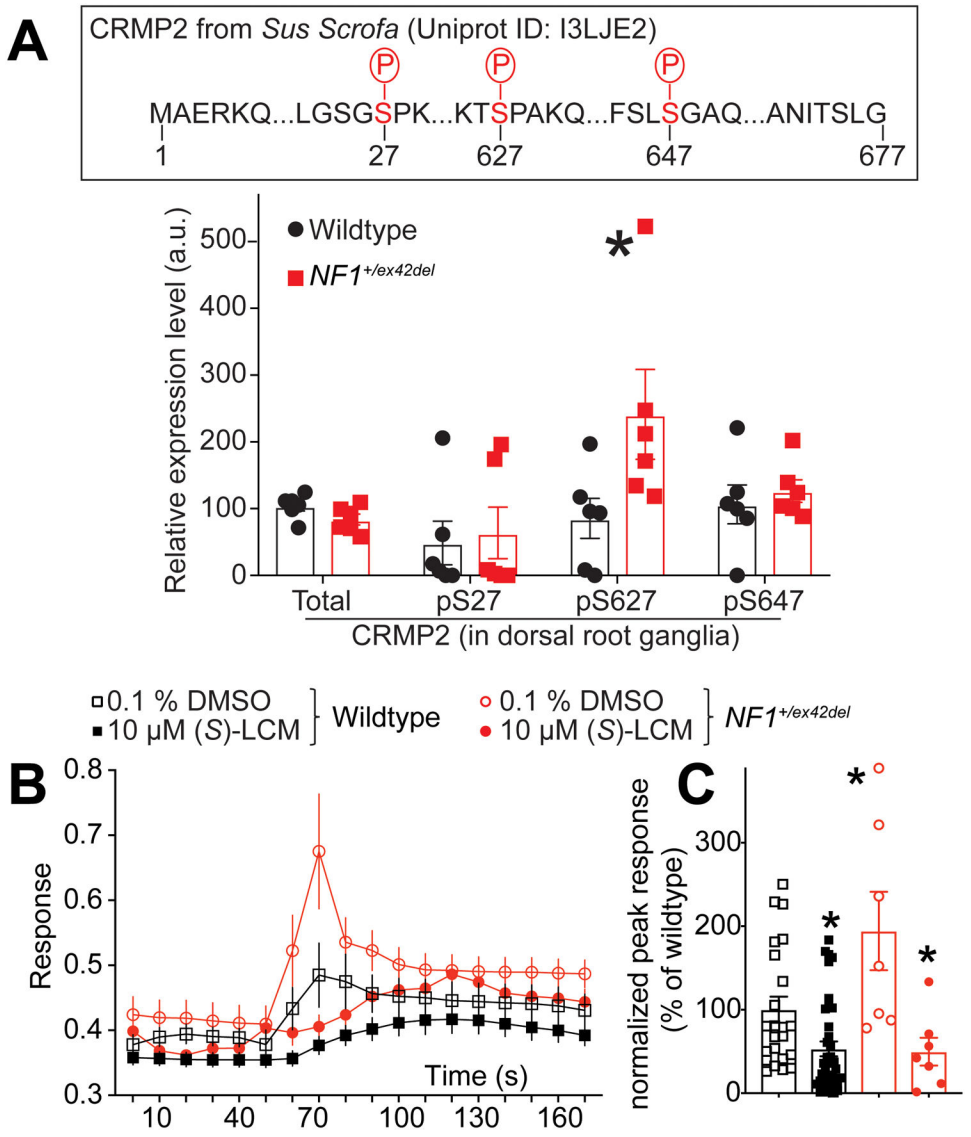

Figure 5. Phosphoproteomic analysis of CRMP2 phosphorylation in *NF1*$^{+/ex42del}$ pig DRGs highlights the potential use of the CRMP2 inhibitor (S)-Lacosamide to decrease depolarization evoked calcium influx.

(**A**) Wildtype or *NF1*$^{+/ex42del}$ pig (female) DRGs whole lysate was analyzed by mass spectrometry for CRMP2 expression and phosphorylation level. The peptide ions m/z was analyzed based on CRMP2 protein sequence from pigs (*sus scrofa*) in Uniprot (I3LJE2). Partial CRMP2 protein sequence is shown and the identified phosphorylation sites highlighted in red. Mass spectrometry returned a quantitative value of peptide abundance compared to the sample load, presented in the bar graph. CRMP2 total expression was unchanged in *NF1*$^{+/ex42del}$ compared to wildtype pig DRGs. Expression level of the phosphorylation sites pS27, pS627 and pS647 was altered in *NF1*$^{+/ex42del}$ pig DRGs. *p<0.05, Mann-Whitney test (n=6 animals per genotype). (**B**) Time course of depolarization evoked calcium influx measured by fura-2 based calcium imaging, in *NF1*$^{+/ex42del}$ or wildtype pig DRG neurons treated with 10 μM of (S)-LCM as indicated. After a 1-min baseline acquisition, calcium influx was evoked by a 15 seconds depolarization using 90

mM KCl. (**C**) Bar graph with scatter plot of peak response (the difference of peak calcium influx normalized to its own baseline for each individual cell) in Pig DRGs treated as indicated. Peak responses were normalized to the wildtype levels for better comparison. Vehicle (0.1% DMSO) or 10 μM (S)-LCM were applied for 30 min prior to depolarization. Peak calcium response was increased in *NF1*$^{+/ex42del}$ pig DRGs compared to wildtype. (S)-LCM treatment inhibited calcium influx in both genotypes. *$p<0.05$ (Mann Whitney) compared to wildtype (0.1 % DMSO).

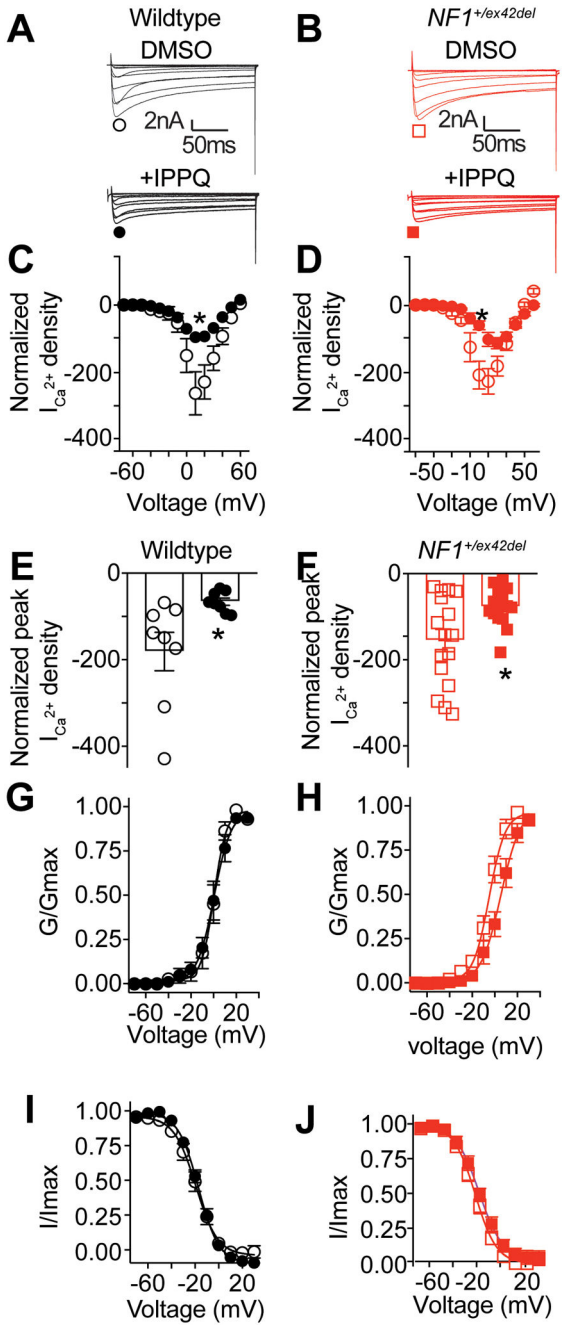

Figure 6: The N-type specific inhibitor IPPQ can decrease calcium currents in wildtype and *NF1*$^{+/ex42del}$ pig DRGs.

Representative traces of calcium currents obtained from (**A**) wildtype or (**B**) *NF1*$^{+/ex42del}$ pig DRGs treated with 20 μM of IPPQ or 0.1 % DMSO (vehicle control) overnight. Curve of current density normalized on the capacitance of each cells and to the level of the DMSO treated control for (**C**) wildtype or (**D**) *NF1*$^{+/ex42del}$ pig DRGs. Bar graph with scatter plot of the peak current density obtained at +10 mV in DRG neurons treated with 20 μM IPPQ overnight compared to vehicle control (0.1 % DMSO) for (**E**) wildtype or (**F**) *NF1*$^{+/ex42del}$ pig DRGs. IPPQ inhibited calcium currents in both genotypes. Activation (G/Gmax) and

inactivation (I/Imax) properties of the calcium currents were not impacted after overnight treatment with IPPQ in both (**G-I**) wildtype and (**H-J**) *NF1*$^{+/ex42del}$ pig DRGs. Graphs show mean ± s.e.m. *p<0.05, Student's t-test.

Table 1.

Description of tumors in the *NF1*$^{+/ex42del}$ pigs.

ID	Sex	DOB	Genotype	Age at Tumor Initiation (mo)	Tumor Description
A6160	Boar	11/18/17	*NF1*$^{+/ex42del}$	7	Small bump on left middle side about 4cm diameter, raised about 0.5cm
A6179	Boar	11/22/17	*NF1*$^{+/ex42del}$	7	Large bump on left side about 11cm x 7cm – raised 1–2cm
A5598	Boar	10/18/17	*NF1*$^{+/ex42del}$	8	One large bump in left middle, odd shaped, about 15cm x 7cm – raised about 2cm; One small bump on right shoulder – about 2cm diameter – raised about 0.5cm
A5664	Boar	10/24/17	*NF1*$^{+/ex42del}$	8	Medium/larger bump on left middle side about 10cm x 5cm – raised about 1cm
A6159	Boar	11/18/17	*NF1*$^{+/ex42del}$	8	Small bump on middle left side about 2 cm in diameter – raised about 0.5cm
A5524	Boar	9/19/17	*NF1*$^{+/ex42del}$	9	small bumps - one L middle side, one L shoulder, both about 2cmx2cm, raised 1 cm
A5725	Boar	11/7/17	*NF1*$^{+/ex42del}$	9	Small bump on right shoulder about 2cm diameter – raised 0.5–1cm
A6173	Boar	11/20/17	*NF1*$^{+/ex42del}$	9	Bump - back L side (has gotten bigger)
A5465	Boar	9/11/17	*NF1*$^{+/ex42del}$	12	Bump - middle of spine
A5601	Boar	10/18/17	*NF1*$^{+/ex42del}$	12	Small bump - back L of spine